

Uranium removal from mining water using Cu substituted hydroxyapatite: Supporting information.

STEPHANIE SZENKNECT[§], ADEL MESBAH[§], MICHAEL DESCOSTES[#], ABDOULAYE MAIHATCHI-AHAMED[§], LAURA BONATO[§], MALVINA MASSONNET[§], YANNIS ZIOUANE[§], EVELYNE VORS[‡], THOMAS VERCOUTER[‡], NICOLAS CLAVIER[§], JOSEPH LAUTRU[§], NICOLAS DACHEUX[§]*

[§] ICSM, CEA, CNRS, ENSCM, Univ Montpellier, Site de Marcoule, BP 17171, 30207 Bagnols/Cèze cedex, France

[#] AREVA Mines, R&D Dpt., Tour AREVA, 1, place Jean Millier, 92084 Paris, La Défense, France

[‡] Den – Service d'Etudes Analytiques et de Réactivité des Surfaces (SEARS), CEA, Université Paris-Saclay, F-91191, Gif sur Yvette, France

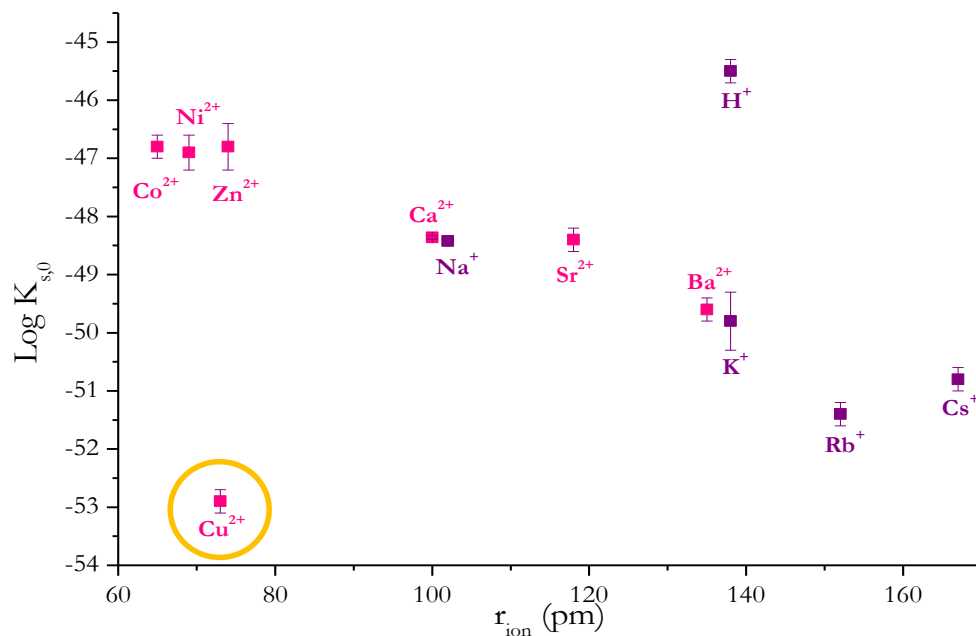


Figure S1. Variation of the standard solubility product $K_{s,0}$ (298.15 K) of phases from the autunite family, $\text{M}^{\text{II}}(\text{UO}_2)_2(\text{PO}_4)_2 \cdot x\text{H}_2\text{O}$ or $\text{M}^{\text{I}}_2(\text{UO}_2)_2(\text{PO}_4)_2 \cdot x\text{H}_2\text{O}$ versus the ionic radius of the incorporated cation.

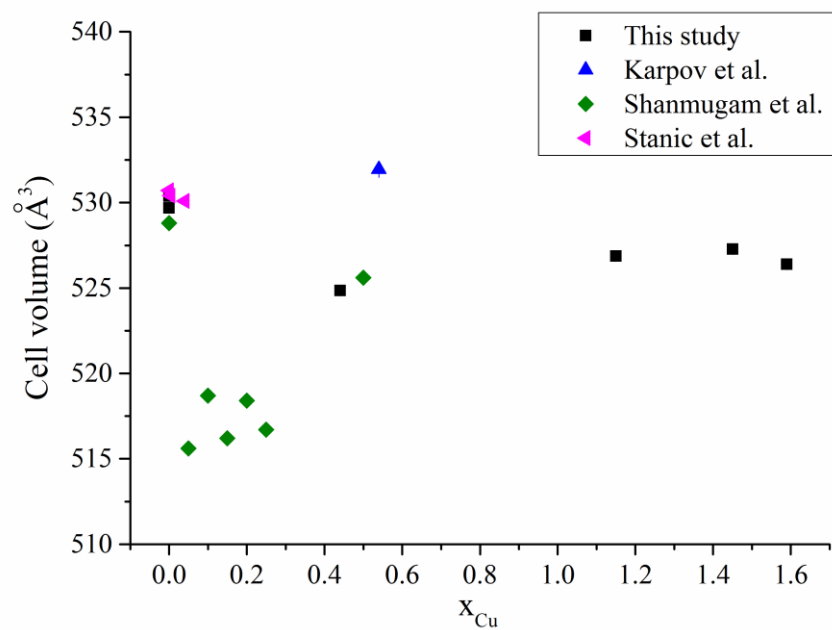
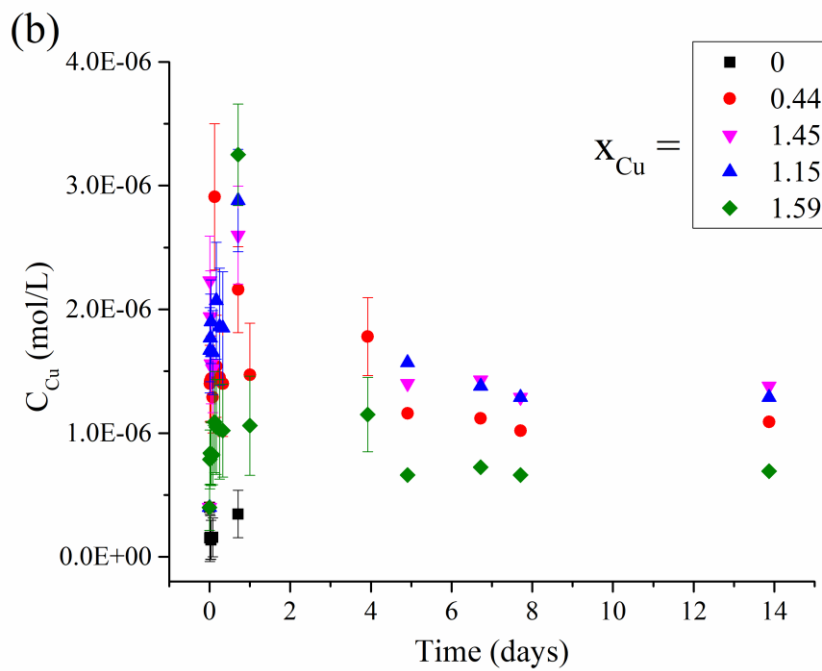
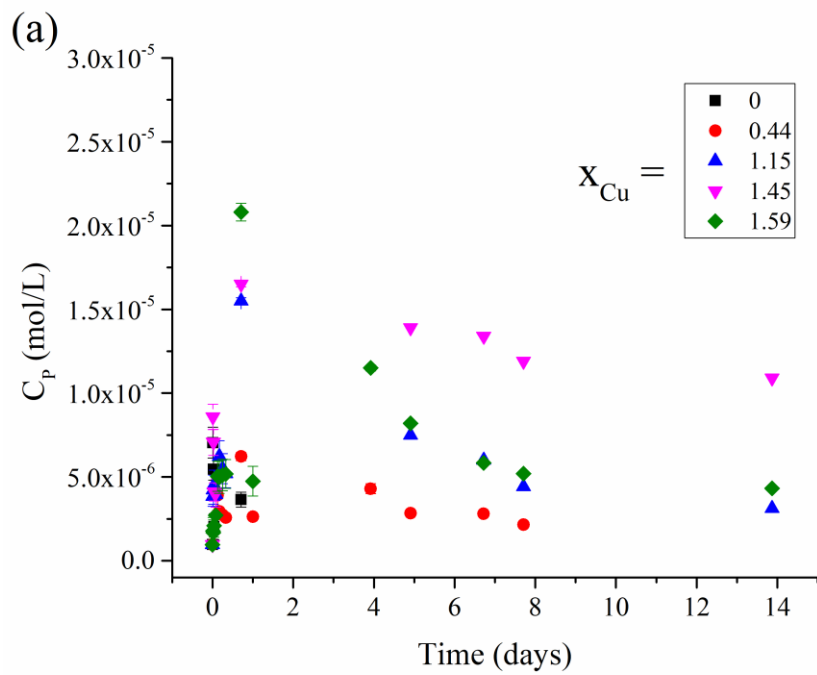


Figure S2. Variation of the cell volume of the Cu-HAP determined by Rietveld refinement of the PXRD patterns. Comparison of the results obtained in this study with ¹⁻⁴.



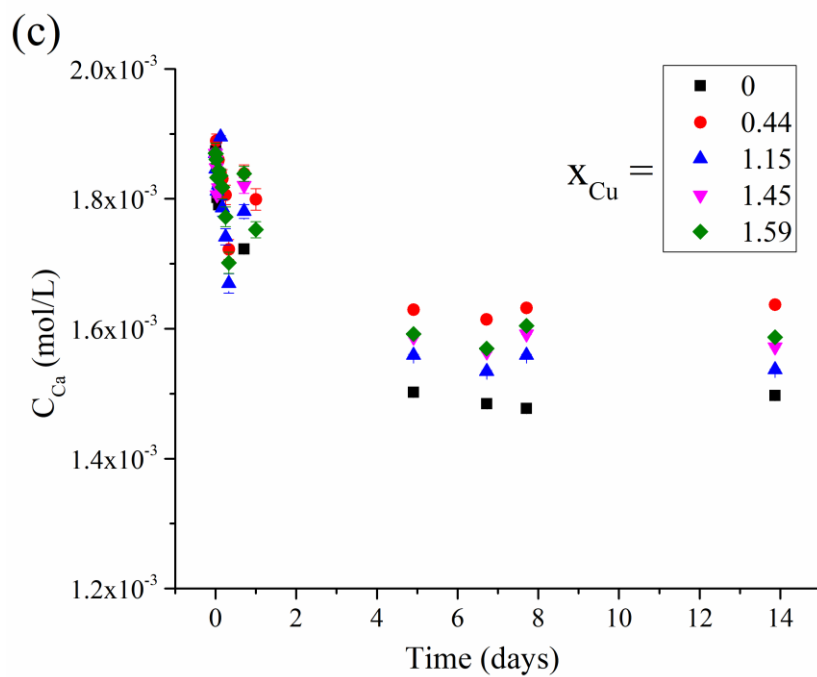
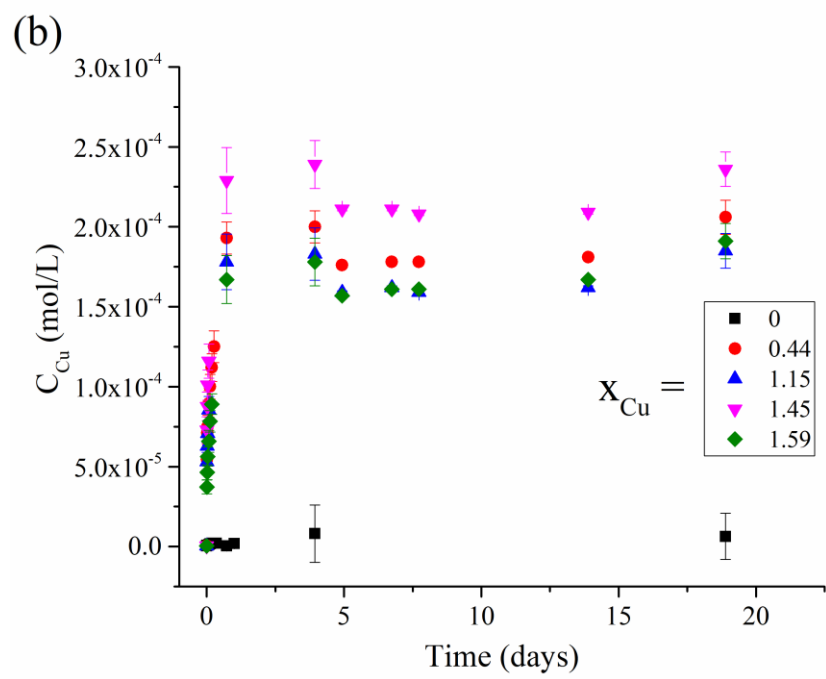
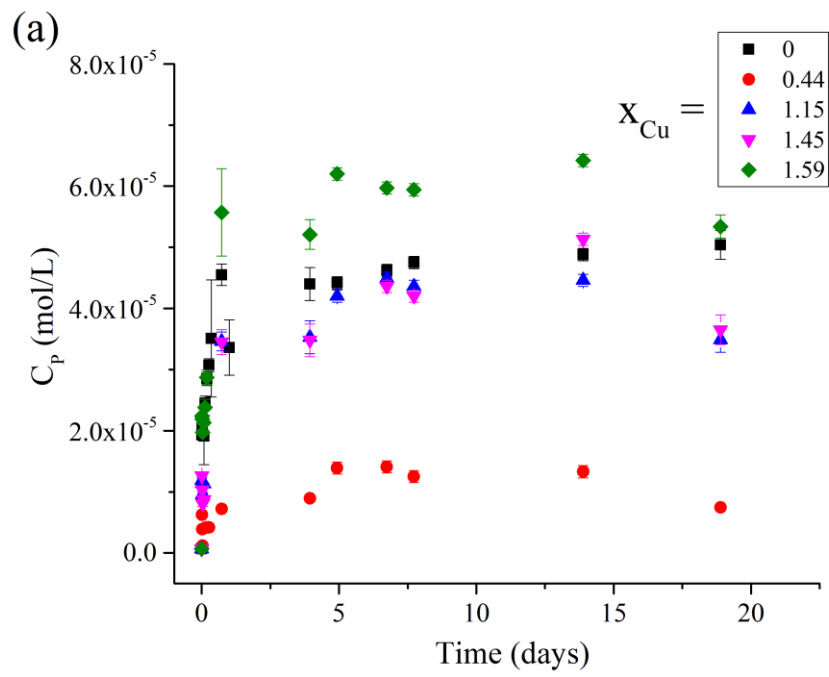


Figure S3. Evolution of the P (a); Cu (b) and Ca (c) elemental concentrations in BD200 mining waters when contacting with the different prepared Cu-Hap samples.



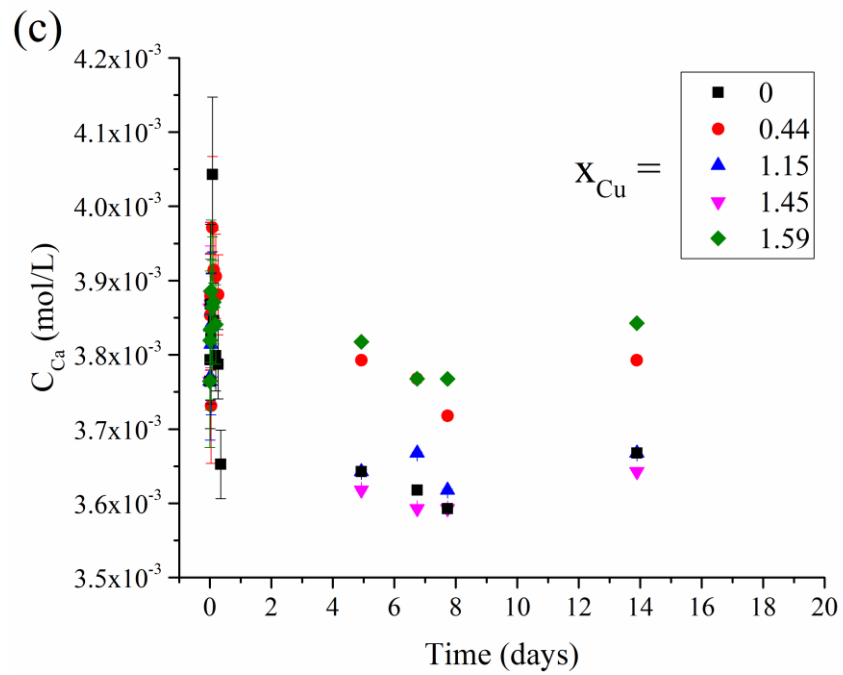


Figure S4. Evolution of the P (a), Cu (b) and Ca (c) elemental concentrations in V105 mining waters when contacting with the different prepared Cu-Hap samples. Ca elemental concentration were

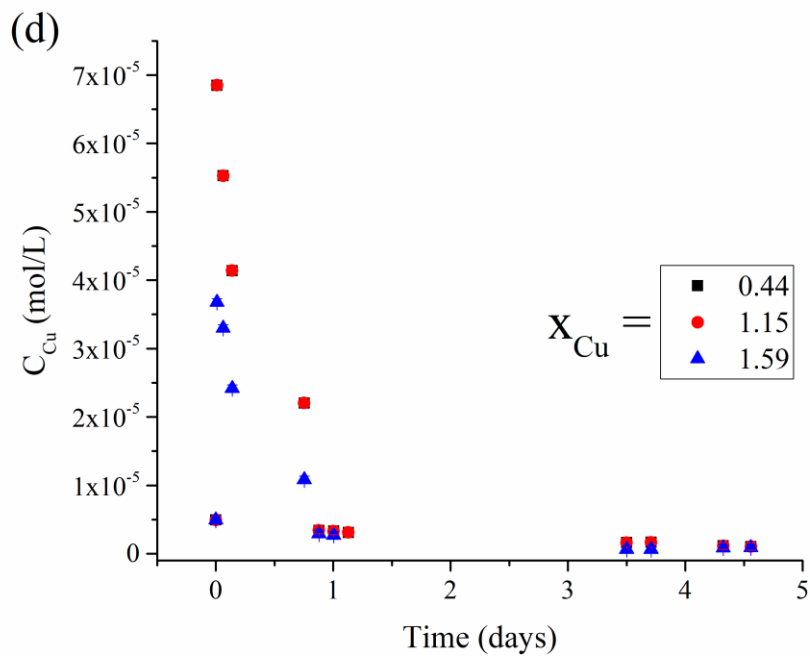
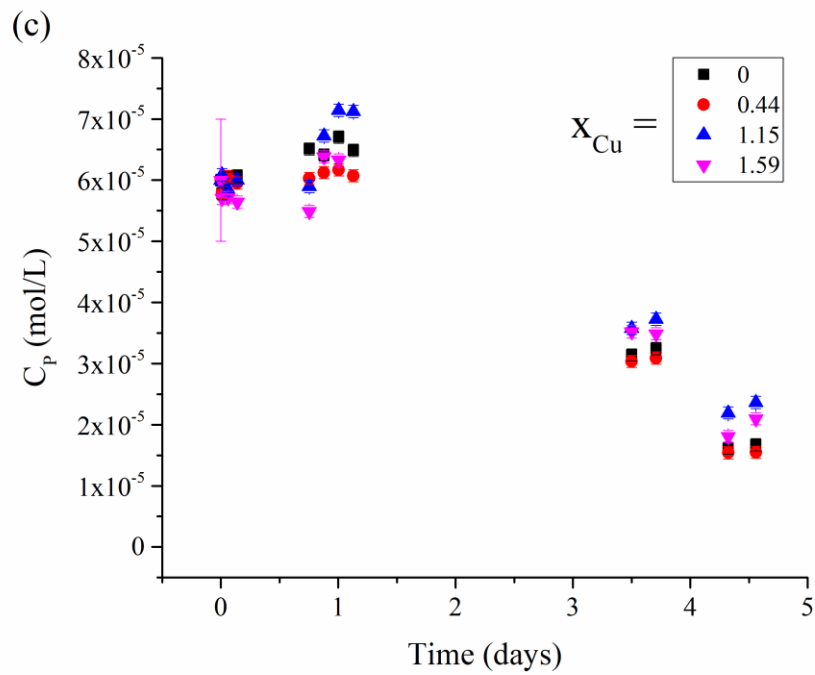
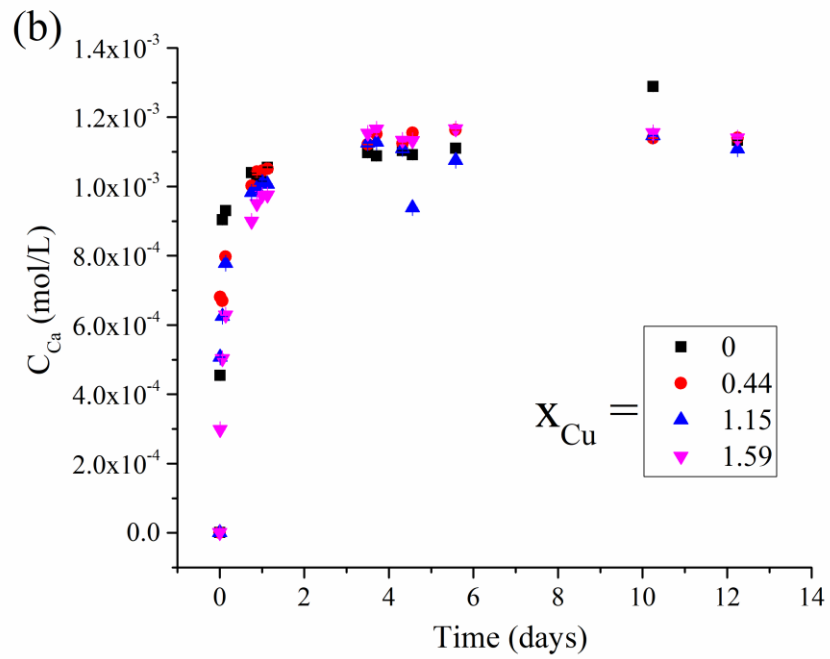
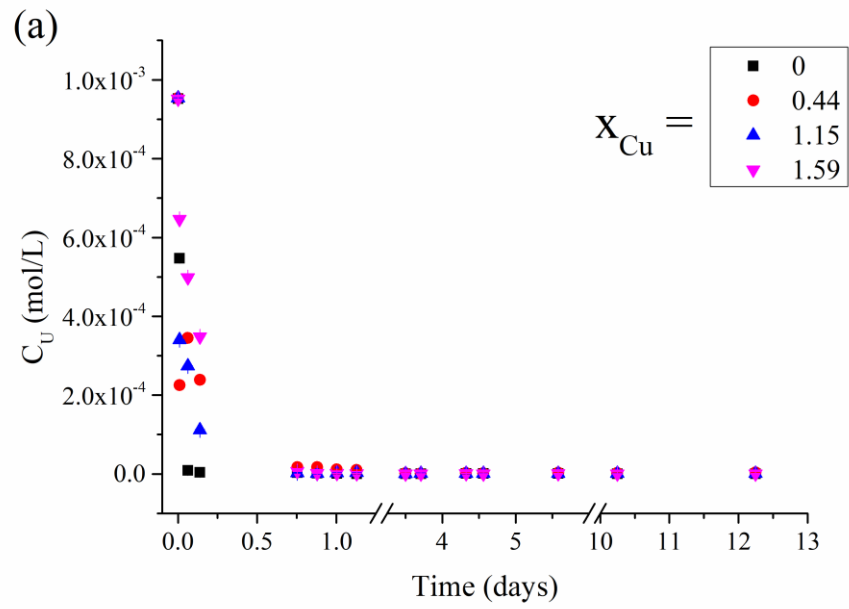


Figure S5. Evolution of the U (a); Ca (b); P (c) and Cu (d) elemental concentrations in spiked synthetic solution of 0.02 mol/L NaNO_3 in contact with the prepared Cu-HAP with various Cu content at near-neutral pH and 25°C.



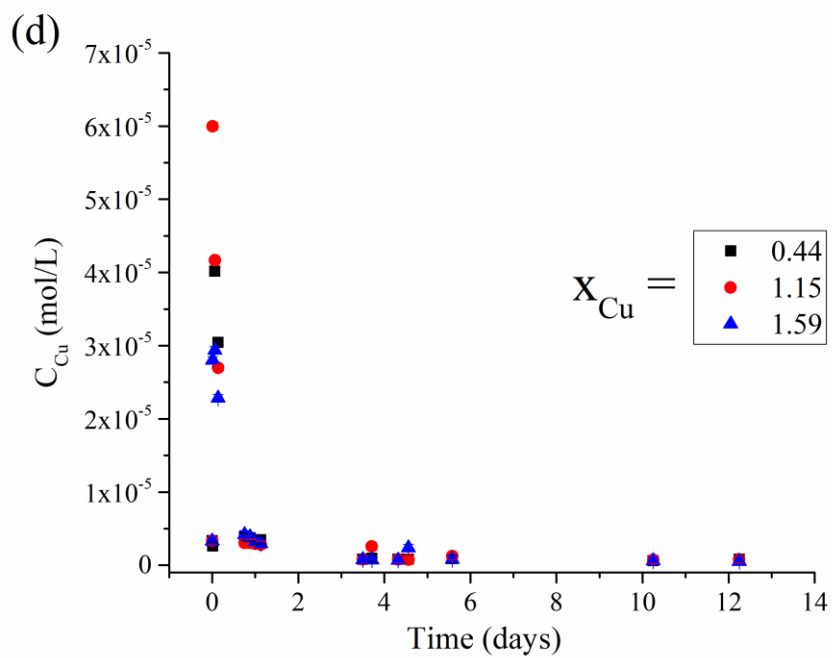
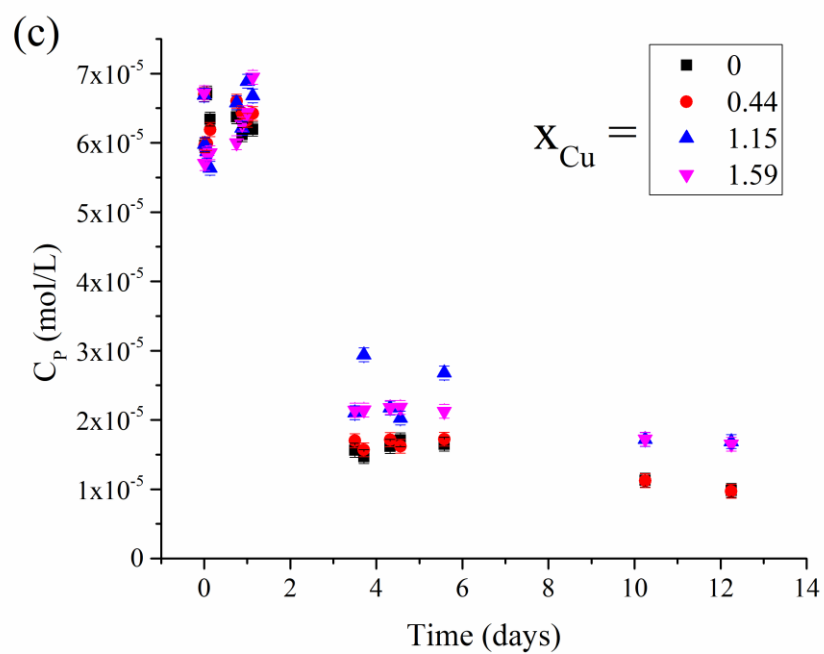
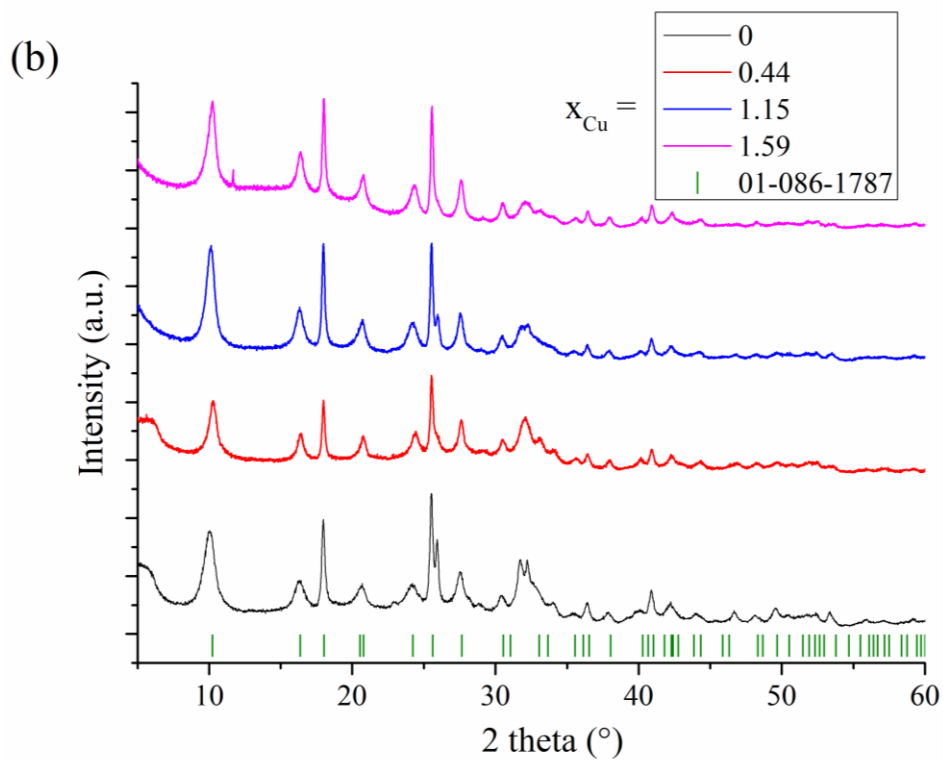
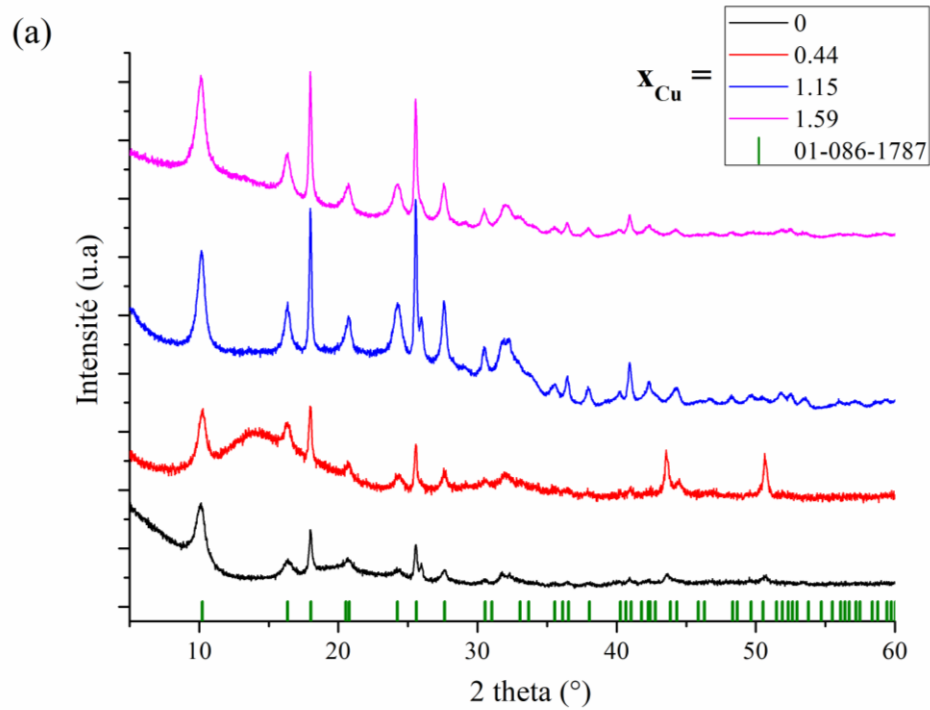


Figure S6. Evolution of the U (a); Ca (b); P (c) and Cu (d) elemental concentrations in uranium spiked synthetic solution of 0.02 mol/L Na_2SO_4 in contact with the prepared Cu-HAP with various Cu content at near-neutral pH and 25°C.



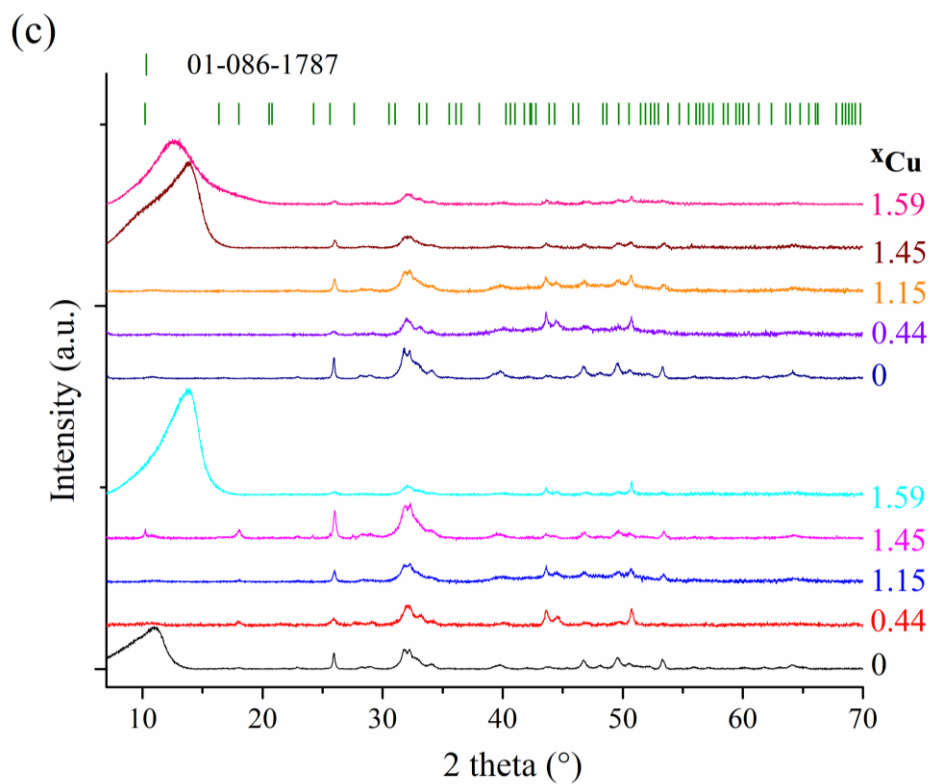


Figure S7. PXRD patterns of Cu-HAP sample after contact with U-spiked ($C_U = 10^{-3}$ mol/L) solution of 0.02 mol/L NaNO_3 (a); Na_2SO_4 (b); V105 and BD200 mining waters ($C_U \sim 10^{-6}$ mol/L) (c). The green bars correspond the Bragg positions of the peaks for meta-torbernite (PDF: 01-086-1787).

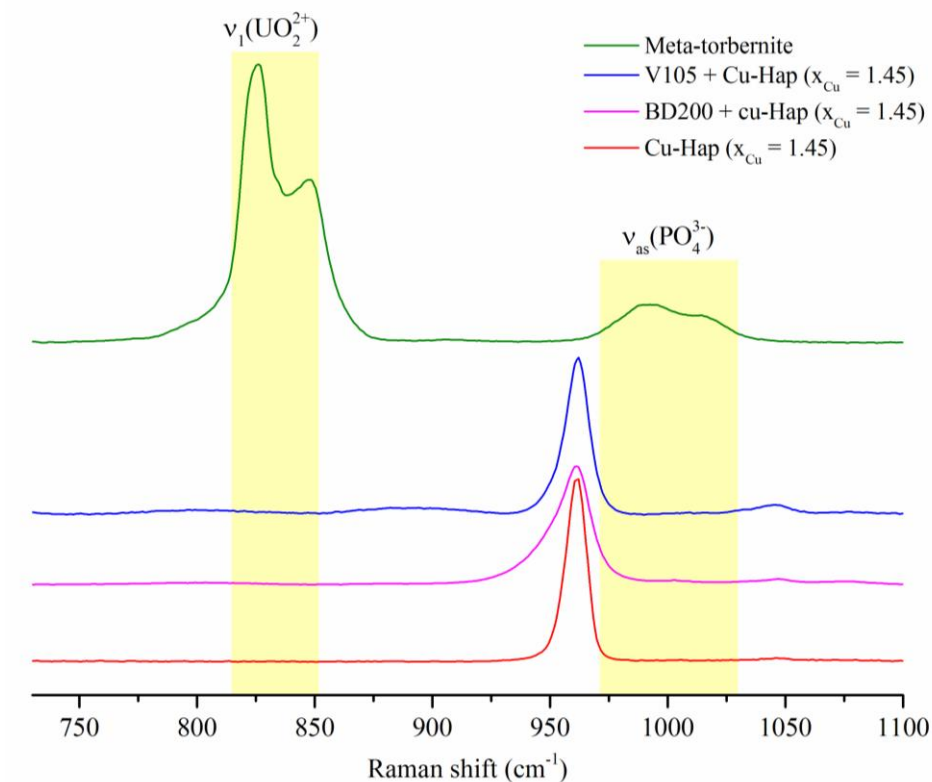
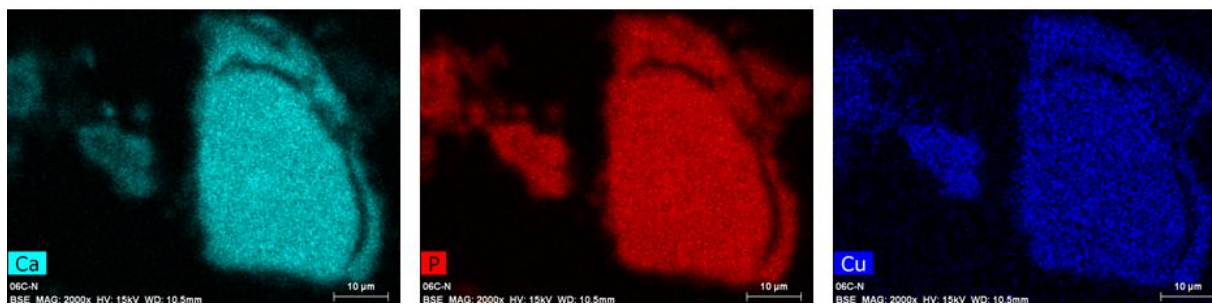
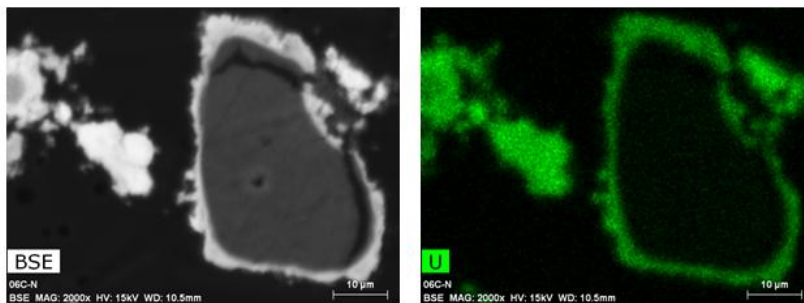


Figure S8. Raman spectra of the Cu-Hap sample ($x_{\text{Cu}} = 1.45$) contacted with BD200 and V105 mining waters compared to the spectrum of the Cu-Hap sample before experiment and with the spectrum of a sample of synthetic meta-torbernite⁵. Attribution of the bands were based on the results obtained by Frost for a natural sample of meta-torbernite⁶.

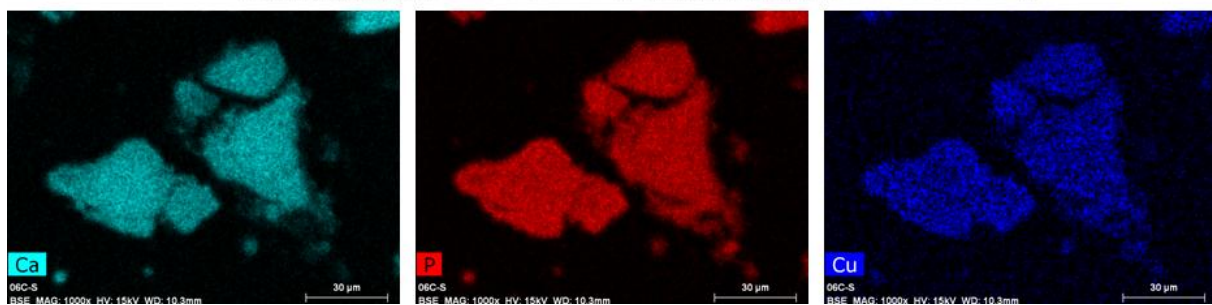
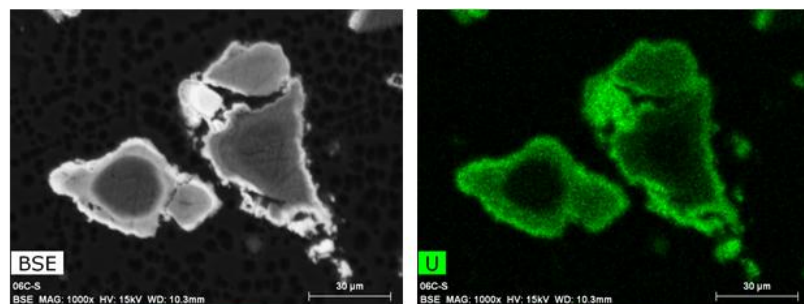
(a)

$x_{Cu} = 1.59$
0.02 M $NaNO_3$



(b)

$x_{Cu} = 1.59$
0.02 M Na_2SO_4



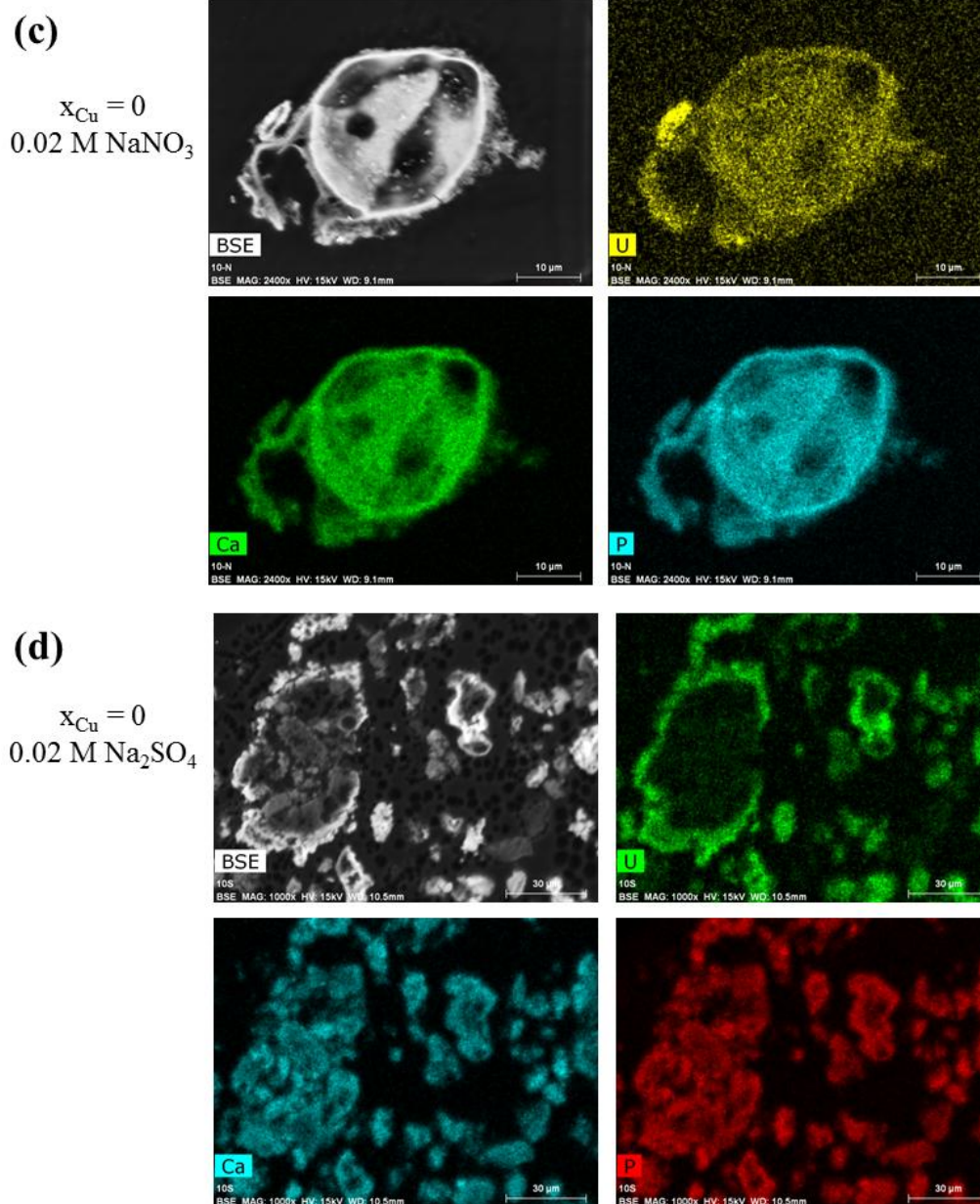


Figure S9. SEM micrograph in backscattered electron mode, U, Ca, Cu and P X-EDS maps determined for Cu-HAP with $x_{\text{Cu}} = 1.59$ contacted with the 0.02 M NaNO_3 solution spiked with uranium (a); with the 0.02 M Na_2SO_4 solution spiked with uranium (b); for Cu-HAP with $x_{\text{Cu}} = 0$ contacted with the 0.02 M NaNO_3 solution spiked with uranium (c); with the 0.02 M Na_2SO_4 solution spiked with uranium (d).

Table S1. Position of the maximum and full width half maximum of TRFLS peaks for Cu-Hap samples contacted with uranyl synthetic solutions and mining waters. Comparison with uranium-bearing synthetic phases of the autunite family.

x_{Cu}	Peak position λ_{max} (nm)				FWHM (nm)
0.02 M Na_2SO_4					
0	502	523	547	572	13
1.15	503	524	547	573	13
1.59	503	524	547	573	13
0.02 M NaNO_3					
0	502	524	547	573	12
1.15	502	524	547	572	14
1.59	502	524	547	572	14
V105					
0	498	519	543	567	13
1.15	497	519	542	567	14
1.45	497	519	542	567	14
BD200					
0	500	521	545	568	15
References	Peak position λ_{max} (nm)				FWHM (nm)
meta-torbernite	502	524	547	573	7
chernikovite	502	524	548	574	7
meta-autunite	502	524	548	573	10

References

1. Karpov, A. S.; Nuss, J.; Jansen, M.; Kazin, P. E.; Tretyakov, Y. D., Synthesis, crystal structure and properties of calcium and barium hydroxyapatites containing copper ions in hexagonal channels. *Solid State Sciences* **2003**, *5*, (9), 1277-1283.
2. Li, C.; Ge, X.; Zhao, J.; Li, G.; Bai, J.; Du, Q.; Ding, R., Preparation and characterization of novel hydroxyapatite/copper assemblies with well-defined morphologies. *Solid State Sciences* **2014**, *29*, 66-74.
3. Shanmugam, S.; Gopal, B., Copper substituted hydroxyapatite and fluorapatite: Synthesis, characterization and antimicrobial properties. *Ceramics International* **2014**, *40*, (10), 15655-15662.
4. Stanic, V.; Dimitrijevic, S.; Antic-Stankovic, J.; Mitric, M.; Jokic, B.; Plecas, I. B.; Raicevic, S., Synthesis, characterization and antimicrobial activity of copper and zinc-doped hydroxyapatite nanopowders. *Applied Surface Science* **2010**, *256*, (20), 6083-6089.
5. Cretaz, F.; Szenknect, S.; Clavier, N.; Vitorge, P.; Mesbah, A.; Descostes, M.; Poinssot, C.; Dacheux, N., Solubility properties of synthetic and natural meta-torbernite. *Journal of Nuclear Materials* **2013**, *442*, (1-3), 195-207.

6. Frost, R. L., An infrared and Raman spectroscopic study of the uranyl micas. *Spectrochimica Acta Part a-Molecular and Biomolecular Spectroscopy* **2004**, *60*, (7), 1469-1480.